ACS APPLIED MATERIALS & INTERFACES

www.acsami.org Research Article

# $MAPbBr_3$ Halide Perovskite-Based Resistive Random-Access Memories Using Electron Transport Layers for Long Endurance Cycles and Retention Time

Hyojung Kim, Joo Sung Kim, Jaeho Choi, Young-Hoon Kim, Jun Min Suh, Min-Ju Choi, Young-Seok Shim, Soo Young Kim, Tae-Woo Lee,* and Ho Won Jang*

Cite This: https://doi.org/10.1021/acsami.3c01450

Read Online

ACCESS | Metrics & More | Article Recommendations | Supporting Information

**ABSTRACT:** Recent studies have focused on exploring the potential of resistive random-access memory (ReRAM) utilizing halide perovskites as novel data storage devices. This interest stems from its notable attributes, including a high ON/OFF ratio, low operating voltages, and exceptional mechanical properties. Nevertheless, there have been reports indicating that memory systems utilizing halide perovskites encounter certain obstacles pertaining to their stability and dependability, mostly assessed through endurance and retention time. Moreover, the presence of these problems can potentially restrict their practical applicability. This study explores a resistive switching memory device utilizing $MAPbBr_3$ perovskite, which demonstrates bipolar switching characteristics. The device fabrication procedure involves a low-temperature, all-solution process. For the purpose of enhancing the device's reliability, the utilization of TPBI(2,2′,2″-(1,3,5-benzinetriyl)-tris(1-phenyl-1-H-benzimidazole) as an electron transfer material on the $MAPbBr_3$ switching layer was implemented for the first time. The formation and rupture of Ag filaments in the $MAPbBr_3$ perovskite switching layer are attributed to reduction−oxidation reactions. The TPBI is involved in the regulation of filaments during the SET and RESET processes. Hence, it can be shown that the $MAPbBr_3$ device incorporating TPBI exhibited about 1000 endurance cycles when subjected to continuous voltage pulses. Moreover, the device consistently maintained ON/OFF ratios above $10^7$. In contrast, the original $MAPbBr_3$ device without TPBI demonstrated a significantly lower endurance with only 90 cycles observed. In addition, the $MAPbBr_3$ device integrated with TPBI exhibited a retention time exceeding $3 \times 10^3$ s. The findings of this research provide compelling evidence to support the notion that electron transfer materials have promise for the development of halide perovskite memory systems owing to their favorable attributes of dependability and stability.

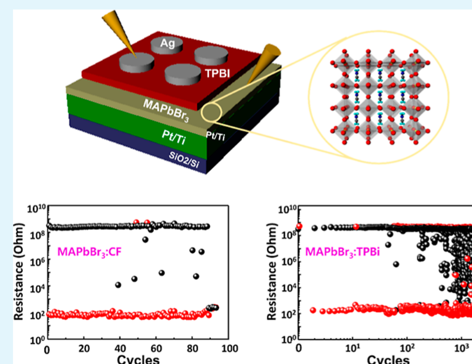


**KEYWORDS:** *resistive random-access memory, $MAPbBr_3$ halide perovskite, electron transport layer, endurance cycles, retention time*

Downloaded via SEOUL NATL UNIV on January 13, 2024 at 13:26:34 (UTC).
See https://pubs.acs.org/sharingguidelines for options on how to legitimately share published articles.

## 1. INTRODUCTION

Resistive random-access memories (ReRAMs) have garnered much attention as a very promising nonvolatile memory technology for future generations. This is mostly due to their numerous advantages, which include low power consumption, rapid switching speed, high integration density, simple architecture, and cost-effectiveness.[1−4] In general, a resistive memory device is composed of a vertical structure known as metal−insulator−metal (MIM), which functions as a two-terminal device. The resistive switching layer, which acts as an insulator, is responsible for establishing a specific resistance state. The resistive switching phenomenon has been seen in several materials, such as chalcogenides,[5] metal oxides,[6] organics,[7] and other substances. Nevertheless, the utilization of low-power and flexible devices has been hindered by certain constraints, mostly stemming from the need for high operating voltage and a high-temperature process.

Recently, there has been a notable surge in interest in halide perovskites. It may be attributed to the fact that photovoltaics has emerged as a promising candidate for meeting future energy demands.[8−11] Halide perovskites possess several desirable characteristics, such as a substantial light absorption coefficient, an extended carrier diffusion length, and a high carrier mobility.[12−15] These attributes have contributed to the heightened attention. The resistive switching property that is particularly considered noteworthy is the current−voltage ($I$−$V$) hysteresis resulting from ion movement.[16] Halide perovskites are compounds with an $ABX_3$ crystal structure, wherein

Received: September 12, 2023
Revised: November 15, 2023
Accepted: November 29, 2023


© XXXX American Chemical Society

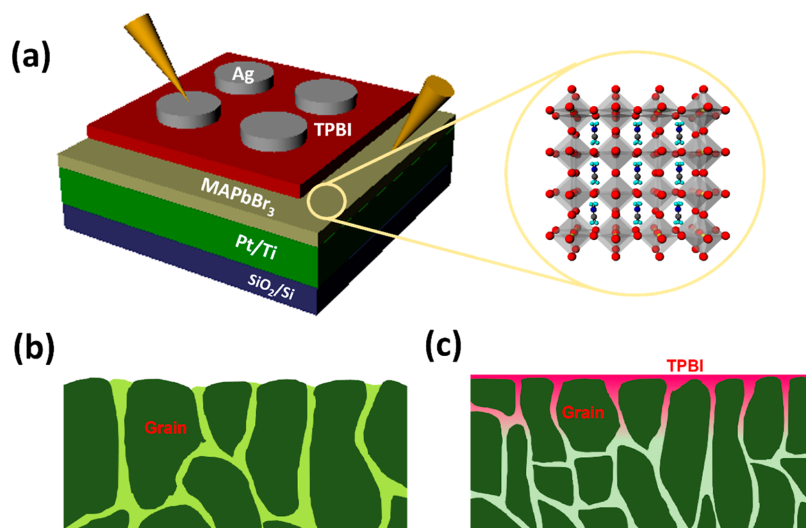


**Figure 1.** (a) Schematic illustration of the resistive memory device structure and resistive switching material, $MAPbBr_3$. Schematic illustrations of $MAPbBr_3$ by CF (b) and $MAPbBr_3$ by TPBI dissolved in CF (c).

the A-site is occupied by monovalent cations such as $CH_3NH_3$ (MA) or Cs, the B-site is occupied by divalent metal cations like Pb or Sn, and the X-site is consistent with halide anions such as I, Br, or Cl.[17,18] In previous studies, researchers have investigated resistive switching memory devices based on $MAPbI_3$, $MAPbBr_3$, or $CsPbI_3$ materials.[19−21] Nevertheless, despite the recognition of halide perovskite-based ReRAM devices as a promising research area, there are still several crucial difficulties that require resolution.

The resistive switching phenomenon occurs by formation and rupture of conducting filaments, accompanied by a complicated redox process. The transition from the initial high resistance state (HRS) to the low resistance state (LRS) at a specific voltage known as the SET voltage signifies the formation of conducting filaments, indicating that the device is in an ON state.[22,23] In accordance with this procedural sequence, the LRS undergoes a transformation to the HRS when subjected to a voltage of opposite polarity, commonly termed the RESET voltage. This transition signifies the attainment of an OFF state.[23,24] However, by the iterative application of a bias polarity or voltage amplitude, conducting filaments undergo a stochastic process of formation and rupture.[25−27] Over time, resistive switching parameters, such as the distribution of ON/OFF ratios, exhibit significant fluctuations, leading to the deterioration of both the switching uniformity and device performance.

In order to tackle these concerns, the utilization of 2,2′,2″-(1,3,5-benzinetriyl)-tris(1-phenyl-1-H-benzimidazole), also known as TPBI, on the halide perovskite layer has been contemplated as a potential approach to improve durability by regulating the growth of the conducting filament. In the context of halide perovskite-based light-emitting diodes (LEDs), TPBI is commonly employed as an electron transport layer (ETL).[28,29] The insertion of a thin layer of TPBI between the resistive switching layer and top electrode is hypothesized to facilitate efficient electron injection into the halide perovskite switching layer. In this study, a resistive switching memory device based on $MAPbBr_3$ was created using a solution processing technique conducted at low temperatures. The utilization of pure chloroform (CF) as an antisolvent resulted in enhanced film uniformity through the reduction of solvent evaporation.[30,31] In order to assess the TPBI layer's reliance, the TPBI compound was dissolved in a solvent known as CF during the execution of the $MAPbBr_3$ crystallization procedure. Both memory devices based on $MAPbBr_3$ had a significant ON/OFF ratio exceeding $1 \times 10^7$ when operated at a speed of 640 $\mu$s and low voltage. In addition, the utilization of TPBI in CF during the synthesis of the $MAPbBr_3$ perovskite resulted in a substantial improvement in its durability, increasing the number of cycles from 90 to over 1000 cycles. Additionally, the perovskite exhibited a large increase in its long-term retention time, extending from 1700 s to $3 \times 10^3$ s.

## 2. EXPERIMENTAL SECTION

**2.1. Materials.** 1,3,5-Tris(2-*N*-phenylbenzimidazolyl) benzene (TPBI) was purchased from OSM, and methylammonium bromide (MABr) was purchased from Greatcell Solar. Lead(II) bromide ($PbBr_2$) (99.999%), dimethyl sulfoxide (DMSO) (99.8%, anhydrous), and CF (99%, anhydrous) were purchased from Sigma-Aldrich. All chemicals were used as received.

**2.2. Fabrication of the Memory Devices.** The 35 wt % of $MAPbBr_3$ precursor solution was prepared by mixing stoichiometric quantities of MABr and $PbBr_2$ in a molar ratio of 1.06:1 (MABr:$PbBr_2$) in DMSO, followed by stirring overnight. A uniform film was obtained by spin-coating the $MAPbBr_3$ precursor on substrates with a speed of 3000 rpm, followed by the nanocrystal pinning method to induce rapid crystallization and uniform morphology by dropping CF during the spin-coating process. For the additive-induced nanocrystal pinning method, 0.1 wt % of TPBI dissolved in CF solution was used instead. After the spin-coating process, the $MAPbBr_3$ film was annealed at 90 °C for 10 min. To complete the devices, Ag electrodes (50 $\mu$m × 50 $\mu$m) were deposited by e-beam evaporation under $1 \times 10^{-6}$ Torr at room temperature through a shadow mask.

**2.3. Characterization.** The surfaces and cross sections of the $MAPbBr_3$ perovskite films were imaged by using a field-emission scanning electron microscope (SUPRA 55VP, Carl Zeiss). The crystal structure of the perovskite films was analyzed by using X-ray photoelectron spectroscopy (XPS) (Korea Basic Science Institute, photon source: monochromatic Al-Ka at 1486.6 eV) and X-ray diffraction (XRD) (Rigaku, D/MAX-2500) measurements. Time-of-flight secondary ion mass spectroscopy (ToF-SIMS) experiments were performed with a ToF-SIMS 5 (ION-TOF GmbH, Münster, Germany) by using a pulsed 30 keV $Bi^+$ primary beam with a current of 0.64 pA. The electrical properties of the memory units were characterized by using an Agilent 4156C semiconductor analyzer in

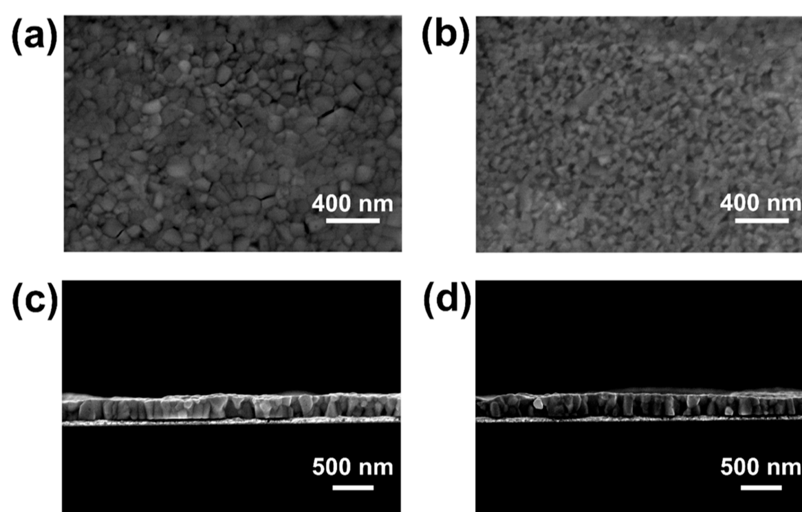


**Figure 2.** Top-view SEM images of the $MAPbBr_3$:CF (a) and $MAPbBr_3$:TPBI (b) films. Cross-sectional SEM images of the $MAPbBr_3$:CF (c) and $MAPbBr_3$:TPBI (d) films.

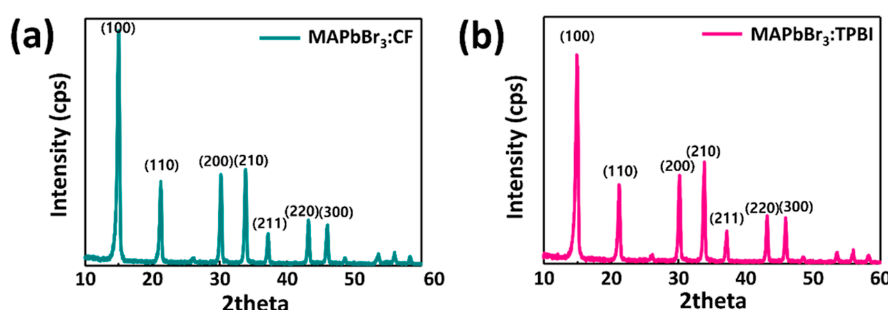


**Figure 3.** XRD pattern in the range of 10−60° of $MAPbBr_3$:CF (a) and $MAPbBr_3$:TPBI (b) films.

the direct current−voltage sweeping mode and alternating voltage pulse mode in a vacuum chamber ($6 \times 10^{-2}$ Torr).

## 3. RESULTS AND DISCUSSION

Figure 1a depicts the vertical stack configuration of silver (Ag) top electrode/TPBI/$MAPbBr_3$/platinum (Pt) bottom electrode/Ti/$SiO_2$/Si. And, the schematic of the crystal structure of the resistive switching material, $MAPbBr_3$, is presented. Metal cations in the form of MA exhibit a pronounced affinity for Br anions, resulting in a rapid and facile crystallization process for $MAPbBr_3$ when employing spin-coating techniques. Therefore, as depicted in Figure 1b,c, the synthesis of $MAPbBr_3$ films was effectively achieved through the utilization of a low-temperature and all-solution approach employing the spin-coating technique. Initially, the precursor solution containing $MAPbBr_3$ was carefully dispensed and evenly distributed on the Pt bottom electrode. Furthermore, the use of CF, a highly volatile nonpolar solvent, involved complete coverage and spin-coating techniques to expedite the evaporation process and facilitate the crystallization of the $MAPbBr_3$ perovskite film.[31] Furthermore, in order to validate the impact of the electron-transporting substance, a solution of TPBI dissolved in CF was applied and dispersed. Following this, Ag top electrodes were applied onto the switching layer using an electron beam evaporator, with a dot-patterned shadow mask employed to delineate the device region (Figure S1).

In order to ascertain the uniformity of these layers, we conducted an examination of the perovskite surfaces. Scanning electron microscopy (SEM) images of $MAPbBr_3$ by CF ($MAPbBr_3$:CF) and $MAPbBr_3$ by TPBI dissolved in CF ($MAPbBr_3$:TPBI) produced on Pt-coated silicon substrates are depicted in Figure 2a,b, respectively. The average grain size of the $MAPbBr_3$:TPBI film exhibited a measurement of around 63.66 nm, showcasing a surface coverage that may be considered flawless. In contrast, the $MAPbBr_3$:CF film had an average grain size of roughly 110.13 nm. According to the data presented in Figure S2a,b, the grain size distribution of $MAPbBr_3$: TPBI exhibited a concentration within the range of 25−100 nm, while the grain size distribution of $MAPbBr_3$:CF displayed a wider range spanning from 50 to 200 nm. There is a suspicion that TPBI may have hindered the formation of crystals in the process of nanocrystal pinning. The presence of TPBI molecules at grain borders has been seen to impede the bonding contact between $MAPbBr_3$ grains during the process of continuous crystallization, leading to a decrease in grain size.[31,32] Figure 2a illustrates the presence of a TPBI layer that is notably thin and partially overlies the surface of $MAPbBr_3$ and its corresponding grain boundary regions. In both instances, the thicknesses of the $MAPbBr_3$ layers measure around 280 nm, as depicted in Figure 2c,d.

XRD was employed to check the crystal structures of $MAPbBr_3$ in both the $MAPbBr_3$:CF and $MAPbBr_3$:TPBI samples. The XRD of the $MAPbBr_3$:CF sample was analyzed within the $2\theta$ range of 10−60°, as depicted in Figure 3a. The pattern exhibited distinct peaks corresponding to the (100), (110), (200), (210), (211), (220), and (300) planes, observed at 15.02, 21.3, 30.28, 33.92, 37.24, 43.28, and 46.00°,



https://doi.org/10.1021/acsami.3c01450
ACS Appl. Mater. Interfaces XXXX, XXX, XXX−XXX

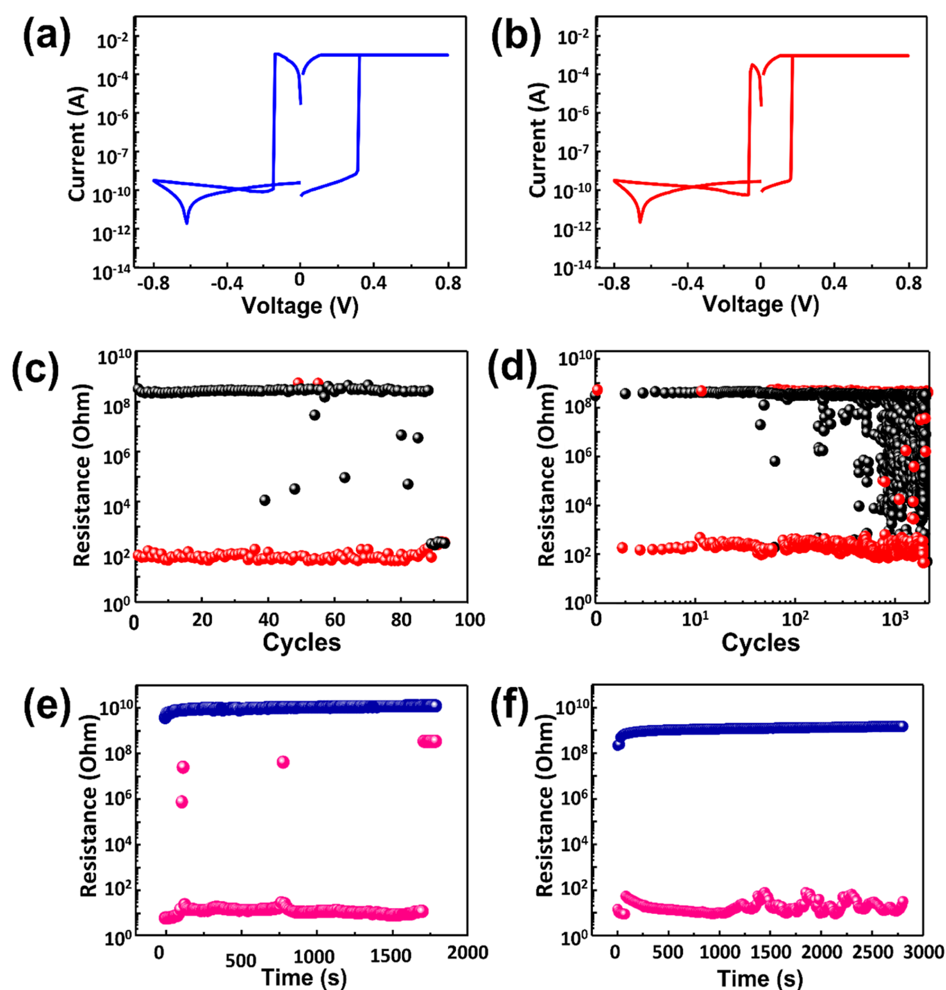


**Figure 4.** Typical *I*−*V* sweeps of the Ag/$MAPbBr_3$/Pt (a) and Ag/TPBI/$MAPbBr_3$/Pt (b) devices. Endurance properties of the Ag/$MAPbBr_3$/Pt (c) and Ag/TPBI/$MAPbBr_3$/Pt (d) devices. Retention time of the Ag/$MAPbBr_3$/Pt (e) and Ag/TPBI/$MAPbBr_3$/Pt (f) devices.

respectively. This observation suggests that the observed patterns exhibit a high degree of conformity with cubic perovskite phases.[33,34] Furthermore, it can be observed from Figure 3b that the peak positions of the $MAPbBr_3$:TPBI film are identical to those of the $MAPbBr_3$:CF film, with no discernible extra or altered peaks. The results suggest that the incorporation of TPBI has no discernible impact on the crystal structures of $MAPbBr_3$ during the process of continuous crystallization.

The programmable switching behaviors of memory devices based on $MAPbBr_3$:CF and $MAPbBr_3$:TPBI have been assessed by *I*−*V* measurements. These measurements were conducted on both devices while subjecting them to a direct current (DC) voltage bias sweep. Figure 4 illustrates the *I*−*V* profiles of the Ag/$MAPbBr_3$/Pt ($MAPbBr_3$:CF) (a) and Ag/TPBI/$MAPbBr_3$/Pt ($MAPbBr_3$:TPBI) (b) device configurations. The voltage was applied to the Ag top electrode, while the Pt bottom electrode was connected to the ground. The electrochemical metallization (ECM) mechanism was seen in the devices. The ECM mechanism entails the formation of a conducting filament that traverses the resistive switching layers, resulting from the oxidation of the active top electrode and subsequent dissolution of the metal cation.[34] Both devices exhibited bipolar resistive switching behavior, characterized by distinct SET and RESET operations, indicating that the ON/OFF states were achieved at opposite polarities.[35−37] In the memory devices based on MAPbBr3:TPBI, as depicted in Figure 4b, a significant transition from a low current state of $1 \times 10^{-10}$ A to a high current state of $1 \times 10^{-3}$ A was observed in the ON state. This transition occurred at a SET operating voltage of +0.15 V. Consequently, the formation of conducting filaments occurs. The sudden rise in current, termed LRS, can be maintained when the device is in the ON state by a compliance current (CC) of $10^{-3}$ A. In order to prevent damage to the device, the current is often restricted by CC during the SET process. Following this, the high current state, which had a current of $1 \times 10^{-3}$ A, was subsequently reduced to the low current state ($10^{-10}$ A) at −0.08 V. The HRS was maintained through the disruption of the conducting filaments during the OFF state. Nevertheless, it has been shown that $MAPbBr_3$:CF devices exhibit marginally elevated and reduced operating voltage when undergoing the SET and RESET processes (Figure 4a), in comparison to $MAPbBr_3$:TPBI devices. The resistive switching phenomenon seen in this memory system can be ascribed to the utilization of TPBI as an electron transport material. The introduction of a TPBI layer over $MAPbBr_3$ enables efficient electron injection into the switching layer, leading to the oxidation of Ag conducting filaments and facilitating the transition to an LRS at lower operating voltages. Moreover, the application of a negative voltage to the device readily triggers the rupture of Ag conducting filaments through the TPBI layer. Therefore, the


https://doi.org/10.1021/acsami.3c01450
ACS Appl. Mater. Interfaces XXXX, XXX, XXX−XXX

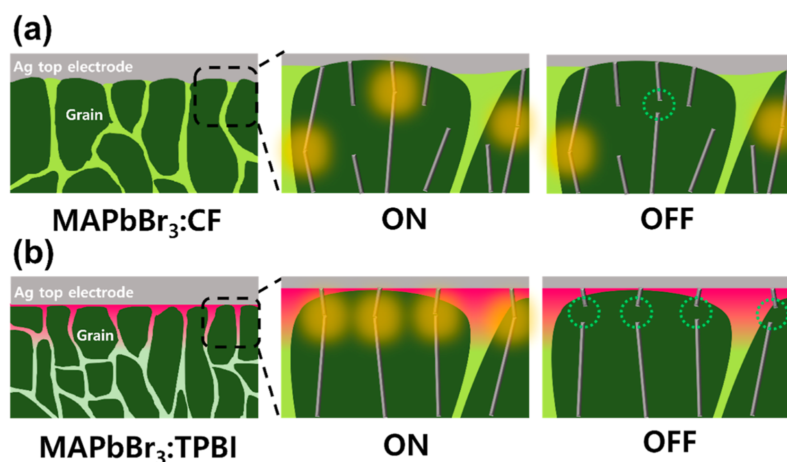


**Figure 5.** ON and OFF mechanisms for the Ag filaments of the Ag/$MAPbBr_3$/Pt ($MAPbBr_3$:CF) (a) and Ag/TPBI/$MAPbBr_3$/Pt ($MAPbBr_3$:TPBI) (b) devices.

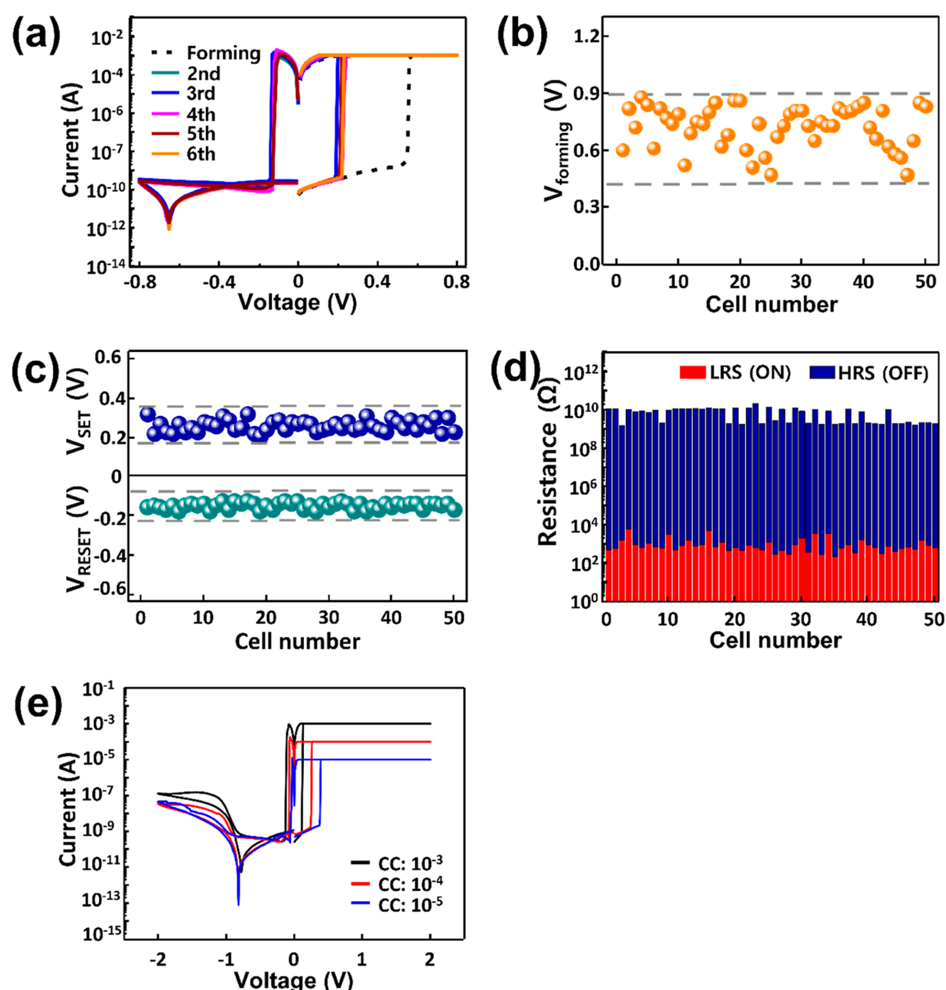


**Figure 6.** (a) Electroforming of Ag/TPBI/$MAPbBr_3$/Pt devices. (b) Forming voltage distribution of Ag/TPBI/$MAPbBr_3$/Pt devices. (c) SET and RESET voltage distributions of Ag/TPBI/$MAPbBr_3$/Pt devices. (d) HRS and LRS for 50 Ag/TPBI/$MAPbBr_3$/Pt cells. (e) Multilevel resistive switching Ag/TPBI/$MAPbBr_3$/Pt devices.

TPBI has the potential to facilitate the formation and rupture of Ag filaments at both lower and higher operating voltages in the SET and RESET processes.

The reliability of the resistive switching memory devices was also evaluated by examining the switching endurance, which is determined by the stability of the number of switching cycles. Figure 4c,d depicts the endurance properties utilized to assess the cycle-to-cycle reproducibility and stability of the $MAPbBr_3$:CF and $MAPbBr_3$:TPBI memory devices, employing alternating current (AC) voltage pulses. The measurement of resistance values involved the application of continuous write-erase pulses with a voltage of +0.8 V for the ON state and −0.8



https://doi.org/10.1021/acsami.3c01450
ACS Appl. Mater. Interfaces XXXX, XXX, XXX−XXX

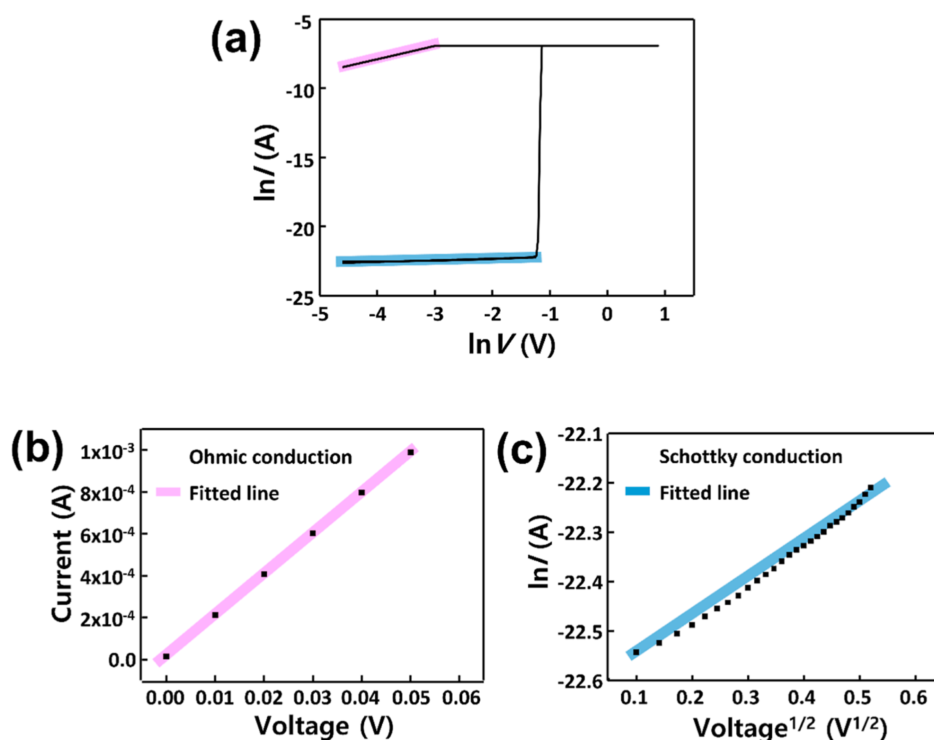


**Figure 7.** (a) Plotted $I$−$V$ curves by double-logarithmic scales (ln $I$ vs ln $V$). (b) Ohmic conduction in the LRS by the linear fitting of the proportional relation of current to the voltage. (c) Replotted ln $I \propto V^{1/2}$ to verify whether Schottky emission is in the HRS region.

V for the OFF state. These were applied during a read voltage of +0.05 V and a pulse duration of 640 $\mu$s. In Figure 4c, it was shown that the $MAPbBr_3$:CF device could endure 90 cycles of HRS and LRS before HRS failure. The observed degradation can be attributed to the random and incomplete RESET occurring at the interface of $MAPbBr_3$.

Nevertheless, as depicted in Figure 4d, the endurance of the $MAPbBr_3$:TPBI memory device was expanded to around 1000 cycles while consistently sustaining ON/OFF ratios above $10^7$. The TPBI between the $MAPbBr_3$ switching layer and Ag top electrode has a significant impact during the RESET process. This interlayer facilitates the injection of electrons, leading to the oxidation of the edges of Ag filaments, ultimately resulting in the rupture of conductive filaments. In order to assess the enhanced resistive switching characteristics of the memory device based on $MAPbBr_3$:TPBI in comparison to prior studies on devices utilizing halide perovskites, the endurance values are presented in Table S1.[16,19,21,36,53,56−69]

In addition, an assessment was conducted on the data retention of the $MAPbBr_3$:CF and $MAPbBr_3$:TPBI memory devices in both the ON and OFF modes. This evaluation was performed at a reading voltage of +0.02 V in order to examine the reliability, as depicted in Figure 4e,f. The $MAPbBr_3$:CF device exhibited a relatively short retention duration, as depicted in Figure 4e. The ON states of the device were initially maintained for a duration of 1700 s. However, these states began to deteriorate and transitioned into the OFF position, resulting in a decreased reliability of the device. Nevertheless, the $MAPbBr_3$:TPBI memory device exhibited a consistent ON/OFF ratio that persisted for a duration exceeding $3 \times 10^3$ s. The small fluctuations were seen in the LRS region, but the ON and OFF states remained quite stable.

To enhance the comprehension of the TPBI roles in $MAPbBr_3$ layers, Figure 5 illustrates the suggested ON and OFF mechanisms pertaining to the behavior of the Ag conducting filaments in the device. The superior resistive switching characteristics seen in the $MAPbBr_3$:TPBI device (Figure 5b) in comparison to those in the $MAPbBr_3$:CF device (Figure 5a) are well accounted for by the presence of TPBI, which is influenced by the efficient electron injection from the Ag/$MAPbBr_3$ interface. Based on the electrochemical metallization theory, the formation of conducting filaments occurs through a series of three phases. First, the Ag top electrode undergoes oxidation electrochemically. Second, the injection of Ag cations takes place, transferring them to the switching layer. Finally, the reduction of the Ag cations occurs, leading to the creation of Ag conducting filaments. During this particular procedure, the introduction of TPBI leads to an augmentation in the electron transport capability. Consequently, this rise prompts the nucleation of Ag atoms and facilitates the creation of conducting filaments at the interface of $MAPbBr_3$.[38−42] Also, the Ag conducting filaments rupture when the negative bias is applied, leading to the migration of Ag cations away from the remaining filaments. In this procedure, the TPBI facilitates the acceleration of filament rupture occurring at the interface of $MAPbBr_3$ by extracting electrons through a negative bias applied to the top electrode.

The resistive switching performance of the $MAPbBr_3$:TPBI device is illustrated in detail in Figure 6. The $I$−$V$ profiles of the $MAPbBr_3$:TPBI device were examined by conducting a set of five sweeps in the DC sweep mode using a semiconductor parameter analyzer, as depicted in Figure 6a. During the initial sweep, an electroforming process, known as a soft breakdown, was detected in the $MAPbBr_3$ layer. This phenomenon demonstrated the ability to achieve stable switching features.[43−45] The process of electroforming was observed in the memory device, wherein a conducting filament bridge was gradually produced until it reached complete formation at a


https://doi.org/10.1021/acsami.3c01450
ACS Appl. Mater. Interfaces XXXX, XXX, XXX−XXX

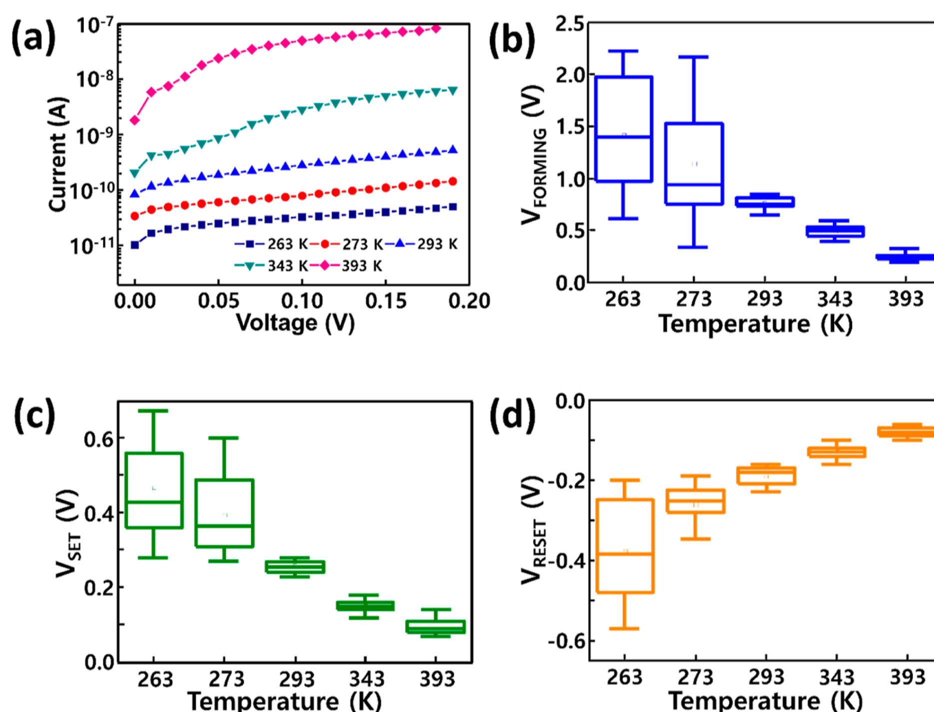


**Figure 8.** Temperature dependence of the HRS before the SET process and tendency of the forming, SET, and RESET voltages with increasing temperature. (a) Temperature dependence of the HRS before the SET process. Tendency of the forming (b), SET (c), and RESET (d) voltages with increasing temperature.

voltage of +0.6 V. Following this particular cycle, the SET process can be conducted at a lower voltage in comparison to the electroforming process. The observed phenomena can be attributed to the pre-existing filament channel that is produced during the electroforming process. This path facilitates the efficient passage of Ag metal cations through the switching layer during the SET operation, even when a low voltage is applied.[34,46,47] In order to assess the operational uniformity of the $MAPbBr_3$:TPBI device, a statistical analysis was conducted on the voltage distributions of formation, SET, and RESET processes for Ag/TPBI/$MAPbBr_3$/Pt cells.

In Figure 6b,c, it is evident that no substantial or relevant variance is observed in the distributions of forming, SET, and RESET voltages across the 50 cells. The HRS and LRS values for a total of 50 cells were measured, as depicted in Figure 6d. Based on the observed distributions, it can be concluded that the ON/OFF values are similar to no significant absolute variations. This finding suggests that the $MAPbBr_3$:TPBI device demonstrates good reproducibility. Furthermore, the capacity of the memory device based on $MAPbBr_3$:TPBI was investigated by tests of its multilevel resistive switching behavior. The purpose of this test was to assess its potential for achieving high data storage density. Three distinct LRS levels are detected in Figure 6e when the CC was varied from $1 \times 10^{-3}$ to $1 \times 10^{-5}$ A. As the CC declined, the resistance value of the LRS decreased. Conversely, there was no observed change in the HRS level with varying CC. The utilization of a $MAPbBr_3$:TPBI device enables the storage of several data levels within a single cell, hence facilitating the expansion of the memory capacity.

To further understand the switching process shown by the MAPbBr3:TPBI device, replotted $I$−$V$ analysis about current transport mechanisms was conducted. Figure 7a displays the $I$−$V$ curves, which were graphed using a double-logarithmic scale (ln $I$ vs ln $V$). Within the LRS range, the $MAPbBr_3$:TPBI device demonstrates Ohmic conduction, characterized by a linear slope of 0.96 after a sudden surge in current.[48−52] Also, the observation of a nonlinear slope of 0.12 suggests that Schottky emission is the prevailing mechanism in the HRS range.[21,53] In order to further understand Ohmic conduction and Schottky emission, the $I$−$V$ curves of the LRS and HRS were reanalyzed. The verification of Ohmic conduction in the LRS is demonstrated by the linear fitting of the $I \propto V$, as seen in Figure 7b.[52] This observation suggests that the Ag conducting filament traverses the $MAPbBr_3$ switching layer after the rapid development of the filaments. Additionally, the $I$−$V$ curve in the HRS area is graphed again using the relationship $\ln I \propto V^{1/2}$. Figure 7c illustrates a plot depicting a linear relationship of $\ln I \propto V^{1/2}$, which serves to demonstrate the dominance of Schottky emission, as defined by the following expression.[53]

$$\ln I \propto \sqrt{\frac{q^3}{4\pi\varepsilon d}kT} \times \sqrt{V} \quad (1)$$

In this context, $I$ represents the current density, $q$ denotes the electric charge, $\varepsilon$ signifies the dielectric constant, $d$ represents the film thickness, $K$ denotes the Boltzmann constant, $T$ represents the absolute temperature, and $V$ denotes the applied voltage. The linear relationship observed in the replotted graph can be attributed to the ability of Ag metal cations to surpass the energy barrier, leading to their dissolution from the Ag top electrode.[54]

To confirm the temperature dependence of the electrical characteristics of the $MAPbBr_3$:TPBI device, we measured the $I$−$V$ test over the temperature range of 263−393 K because the electrochemical reactions and thermal effects contribute to the development and rupture of filaments in the device. As depicted in Figure 8a, the HRS current elevates as temperature

increases, which demonstrates that the Ag cations readily migrate toward the $MAPbBr_3$ layer subsequent to the dissolution of the Ag metal electrode.[21,36,53] Also, the *I*−*V* curves depicted in Figure S3 demonstrate that TPBI used perovskite devices that displayed Ohmic contact characteristics, as seen by the exponential plots. These plots revealed a linear slope of 1 inside the LRS region across different temperatures. Figure 8b,c illustrates the declining patterns observed in the forming and SET voltages as the temperature increases. During the process of formation and subsequent SET operation, Ag cations easily move through the $MAPbBr_3$ layer. This migration enables them to rapidly achieve a state of supersaturation at the Pt counter electrode, hence resulting in a reduction in the operating voltages.[36,53,55] In Figure 8d, a positive correlation is shown between the RESET voltages and temperature, indicating an increasing trend. The occurrence of the rupture of the conducting filament during the RESET operation might be attributed to the process of dissolution, which is facilitated by Joule heating.[36,37,55] The Ag conducting filaments, which exhibit thermal instability, are susceptible to fracture when exposed to elevated temperatures. Therefore, it is seen that the Ag filament exhibits a high susceptibility to disconnection even when subjected to a low-intensity electric field.

## 4. CONCLUSIONS

To summarize, the utilization of TPBI, an electron transfer material, was implemented in the incorporation of $MAPbBr_3$ to enhance the endurance cycles and the retention time. The introduction of a TPBI layer between the Ag top electrode and the $MAPbBr_3$ switching layer resulted in the achievement of a uniform surface. This incorporation significantly improved the resistive switching properties. The resistive switching characteristics seen in the Ag/TPBI/$MAPbBr_3$/Pt device are attributed to the formation and rupture of Ag conducting filaments within the $MAPbBr_3$ layer. Both memory devices based on $MAPbBr_3$ had a significant ON/OFF ratio exceeding $10^7$ when operated at a speed of 640 $\mu$s and low voltage. The endurance of the $MAPbBr_3$:TPBI device was observed to be approximately 1000 cycles, a much greater value compared to the endurance cycles of the $MAPbBr_3$:CF memory device. The TPBI facilitates the efficient injection of electrons into the switching layer. As a result, the oxidation process of Ag conducting filaments is enhanced, leading to an improved efficiency in the rupture of these filaments. Furthermore, an assessment was conducted to examine the reliability of the memory device by evaluating the retention time. A continuous alternation between an ON and OFF state was sustained for a duration exceeding $3 \times 10^3$ s. Therefore, our study holds significance in relation to providing an alternative approach to enhance the switching capability of halide perovskite memory devices.

## ■ ASSOCIATED CONTENT

### Supporting Information

The Supporting Information is available free of charge at https://pubs.acs.org/doi/10.1021/acsami.3c01450.

Optical microscopy images of $MAPbBr_3$ resistive switching memory devices and grain size distribution of $MAPbBr_3$:CF and $MAPbBr_3$:TPBI films (PDF)

## ■ AUTHOR INFORMATION


### Corresponding Authors

**Tae-Woo Lee** − *Department of Materials Science and Engineering Seoul National University, Seoul 08826, Republic of Korea*; orcid.org/0000-0002-6449-6725; Email: twlees@snu.ac.kr

**Ho Won Jang** − *Department of Materials Science and Engineering Seoul National University, Seoul 08826, Republic of Korea*; orcid.org/0000-0002-6952-7359; Email: hwjang@snu.ac.kr

### Authors

**Hyojung Kim** − *Department of Materials Science and Engineering Seoul National University, Seoul 08826, Republic of Korea; Davidson School of Chemical Engineering, Purdue University, West Lafayette, Indiana 47907, United States; Department of Semiconductor Systems Engineering, Sejong University, Seoul 05006, Republic of Korea*

**Joo Sung Kim** − *Department of Materials Science and Engineering Seoul National University, Seoul 08826, Republic of Korea*

**Jaeho Choi** − *Department of Materials Science and Engineering Seoul National University, Seoul 08826, Republic of Korea*

**Young-Hoon Kim** − *Department of Materials Science and Engineering Seoul National University, Seoul 08826, Republic of Korea; Department of Energy Engineering, Hanyang University, Seoul 04763, Republic of Korea*

**Jun Min Suh** − *Department of Mechanical Engineering, Massachusetts Institute of Technology, Cambridge, Massachusetts 02139, United States*

**Min-Ju Choi** − *Department of Materials Science and Engineering Seoul National University, Seoul 08826, Republic of Korea*

**Young-Seok Shim** − *School of Energy, Materials and Chemical Engineering, Korea University of Technology and Education, Cheonan 31253, Republic of Korea*

**Soo Young Kim** − *Department of Materials Science and Engineering, Korea University, Seoul 02841, Republic of Korea*; orcid.org/0000-0002-0685-7991

Complete contact information is available at: https://pubs.acs.org/10.1021/acsami.3c01450


### Notes

The authors declare no competing financial interest.

## ■ ACKNOWLEDGMENTS


This work was financially supported by the Future Material Discovery Program (2016M3D1A1027666, 2018M3D1A1058793, 2016R1A3B1908431, and 2022H1D3A3A01081288) and the Nano Material Technology Development Program (2022M3H4A1A01011963) through the National Research Foundation of Korea. Also, this research was supported by the Basic Science Research Program through the National Research Foundation of Korea funded by the Ministry of Education (2021R1A6A3A1404499113) and grants funded by the Korea government (MSIT) (2022R1A5A1032539 and 2022R1C1C1008282). Also, this work was supported by the faculty research fund of Sejong University in 2023.

## ■ REFERENCES


(1) Su, Z. S.; Fung, M. K.; Lee, C. S.; Li, W. L.; Lee, S. T. Memory Effect and Negative Differential Resistance in Tris-(8-Hydroxy Quinoline) Aluminum/Bathocuproine Bilayer Devices. *Appl. Phys. Lett.* **2008**, *93* (8), 083301.
(2) Joshua Yang, J.; Miao, F.; Pickett, M. D.; Ohlberg, D. A. A.; Stewart, D. R.; Lau, C. N.; Williams, R. S. The Mechanism of Electroforming of Metal Oxide Memristive Switches. *Nanotechnology* **2009**, *20* (21), 215201.
(3) Yasuhara, R.; Yamamoto, T.; Ohkubo, I.; Kumigashira, H.; Oshima, M. Interfacial Chemical States of Resistance-Switching Metal/Pr0.7 Ca0.3MnO3 Interfaces. *Appl. Phys. Lett.* **2010**, *97* (13), 132111.
(4) Jiang, A. Q.; Wang, C.; Jin, K. J.; Liu, X. B.; Scott, J. F.; Hwang, C. S.; Tang, T. A.; Lu, H. bin; Yang, G. Z. A Resistive Memory in Semiconducting BiFeO3 Thin-Film Capacitors. *Adv. Mater.* **2011**, *23* (10), 1277−1281.
(5) van den Hurk, J.; Valov, I.; Waser, R. Preparation and Characterization of GeSx Thin-Films for Resistive Switching Memories. *Thin Solid Films* **2013**, *527*, 299−302.
(6) Huang, Y.; Shen, Z.; Wu, Y.; Wang, X.; Zhang, S.; Shi, X.; Zeng, H. Amorphous ZnO Based Resistive Random Access Memory. *RSC Adv.* **2016**, *6* (22), 17867−17872.
(7) Song, S.; Cho, B.; Kim, T. W.; Ji, Y.; Jo, M.; Wang, G.; Choe, M.; Kahng, Y. H.; Hwang, H.; Lee, T. Three-Dimensional Integration of Organic Resistive Memory Devices. *Adv. Mater.* **2010**, *22* (44), 5048−5052.
(8) Kim, H.; Veerappan, G.; Park, J. H. Conducting Polymer Coated Non-Woven Graphite Fiber Film for Dye-Sensitized Solar Cells: Superior Pt- and FTO-Free Counter Electrodes. *Electrochim. Acta* **2014**, *137*, 164−168.
(9) Kim, H.; Veerappan, G.; Wang, D. H.; Park, J. H. Large Area Platinum and Fluorine-Doped Tin Oxide-Free Dye Sensitized Solar Cells with Silver-Nanoplate Embedded Poly(3,4-Ethylenedioxythiophene) Counter Electrode. *Electrochim. Acta* **2016**, *187*, 218−223.
(10) Jo, J. W.; Yoo, Y.; Jeong, T.; Ahn, S. J.; Ko, M. J. Low-Temperature Processable Charge Transporting Materials for the Flexible Perovskite Solar Cells. *Electron. Mater. Lett.* **2018**, *14* (6), 657−668.
(11) Green, M. A.; Ho-Baillie, A.; Snaith, H. J. The Emergence of Perovskite Solar Cells. *Nat. Photonics* **2014**, *8* (7), 506−514.
(12) Mitzi, D. B. Templating and Structural Engineering in Organic-Inorganic Perovskites. *J. Chem. Soc., Dalton Trans.* **2001**, No. 1, 1−12.
(13) Quan, L. N.; Yuan, M.; Comin, R.; Voznyy, O.; Kim, D. H.; Sargent, E. H. *Quasi-2D Perovskites for Efficient Solar Cells and LEDs*; SPIE Newsroom, 2016, .
(14) Kieslich, G.; Sun, S.; Cheetham, A. K. Solid-State Principles Applied to Organic-Inorganic Perovskites: New Tricks for an Old Dog. *Chem. Sci.* **2014**, *5* (12), 4712−4715.
(15) Chen, Q.; De Marco, N.; Yang, Y.; Song, T. B.; Chen, C. C.; Zhao, H.; Hong, Z.; Zhou, H.; Yang, Y. Under the Spotlight: The Organic-Inorganic Hybrid Halide Perovskite for Optoelectronic Applications. *Nano Today* **2015**, *10* (3), 355−396.
(16) Gu, C.; Lee, J. S. Flexible Hybrid Organic-Inorganic Perovskite Memory. *ACS Nano* **2016**, *10* (5), 5413−5418.
(17) Kim, H.; Han, J. S.; Choi, J.; Kim, S. Y.; Jang, H. W. Halide Perovskites for Applications beyond Photovoltaics. *Small Methods* **2018**, *2* (3), 1700310.
(18) Kim, H.; Huynh, K. A.; Kim, S. Y.; Le, Q. V.; Jang, H. W. 2D and Quasi-2D Halide Perovskites: Applications and Progress. *Phys. Status Solidi RRL* **2020**, *14* (2), 1900435.
(19) Choi, J.; Park, S.; Lee, J.; Hong, K.; Kim, D. H.; Moon, C. W.; Park, G. do; Suh, J.; Hwang, J.; Kim, S. Y.; Jung, H. S.; Park, N. G.; Han, S.; Nam, K. T.; Jang, H. W. Organolead Halide Perovskites for Low Operating Voltage Multilevel Resistive Switching. *Adv. Mater.* **2016**, *28* (31), 6562−6567.
(20) Hwang, B.; Gu, C.; Lee, D.; Lee, J. S. Effect of Halide-Mixing on the Switching Behaviors of Organic-Inorganic Hybrid Perovskite Memory. *Sci. Rep.* **2017**, *7*, 43794.
(21) Han, J. S.; Le, Q. v.; Choi, J.; Hong, K.; Moon, C. W.; Kim, T. L.; Kim, H.; Kim, S. Y.; Jang, H. W. Air-Stable Cesium Lead Iodide Perovskite for Ultra-Low Operating Voltage Resistive Switching. *Adv. Funct. Mater.* **2018**, *28* (5), 1705783.
(22) Pan, F.; Gao, S.; Chen, C.; Song, C.; Zeng, F. Recent Progress in Resistive Random Access Memories: Materials, Switching Mechanisms, and Performance. *Mater. Sci. Eng., R* **2014**, *83* (1), 1−59.
(23) Kim, H.; Han, J. S.; Kim, S. G.; Kim, S. Y.; Jang, H. W. Halide Perovskites for Resistive Random-Access Memories. *J. Mater. Chem. C* **2019**, *7* (18), 5226−5234.
(24) Wang, J. C.; Ye, Y. R.; Lai, C. S.; Lin, C. T.; Lu, H. C.; Wu, C. I.; Wang, P. S. Characterization of Gadolinium Oxide Thin Films with CF 4 Plasma Treatment for Resistive Switching Memory Applications. *Appl. Surf. Sci.* **2013**, *276*, 497−501.
(25) Nandakumar, S. R.; Minvielle, M.; Nagar, S.; Dubourdieu, C.; Rajendran, B. A 250 MV Cu/SiO2/W Memristor with Half-Integer Quantum Conductance States. *Nano Lett.* **2016**, *16* (3), 1602−1608.
(26) Liu, Q.; Long, S.; Lv, H.; Wang, W.; Niu, J.; Huo, Z.; Chen, J.; Liu, M. Controllable Growth of Nanoscale Conductive Filaments in Solid-Electrolyte-Based ReRAM by Using a Metal Nanocrystal Covered Bottom Electrode. *ACS Nano* **2010**, *4* (10), 6162−6168.
(27) Ninomiya, T.; Wei, Z.; Muraoka, S.; Yasuhara, R.; Katayama, K.; Takagi, T. Conductive Filament Scaling of ${\rm TaO}_{\rm x}$ Bipolar ReRAM for Improving Data Retention Under Low Operation Current. *IEEE Trans. Electron Devices* **2013**, *60* (4), 1384−1389.
(28) Yang, X.; Divayana, Y.; Zhao, D.; Swee Leck, K.; Lu, F.; Tiam Tan, S.; Putu Abiyasa, A.; Zhao, Y.; Volkan Demir, H.; Wei Sun, X. A Bright Cadmium-Free, Hybrid Organic/Quantum Dot White Light-Emitting Diode. *Appl. Phys. Lett.* **2012**, *101* (23), 233110.
(29) Perumal, A.; Shendre, S.; Li, M.; Tay, Y. K. E.; Sharma, V. K.; Chen, S.; Wei, Z.; Liu, Q.; Gao, Y.; Buenconsejo, P. J. S.; Tan, S. T.; Gan, C. L.; Xiong, Q.; Sum, T. C.; Demir, H. V. High Brightness Formamidinium Lead Bromide Perovskite Nanocrystal Light Emitting Devices. *Sci. Rep.* **2016**, *6*, 36733.
(30) Wu, C.; Zou, Y.; Wu, T.; Ban, M.; Pecunia, V.; Han, Y.; Liu, Q.; Song, T.; Duhm, S.; Sun, B. Improved Performance and Stability of All-Inorganic Perovskite Light-Emitting Diodes by Antisolvent Vapor Treatment. *Adv. Funct. Mater.* **2017**, *27* (28), 1700338.
(31) Cho, H.; Jeong, S.-H.; Park, M.-H.; Kim, Y.-H.; Wolf, C.; Lee, C.-L.; Heo, J. H.; Sadhanala, A.; Myoung, N.; Yoo, S.; Im, S. H.; Friend, R. H.; Lee, T.-W. Overcoming the Electroluminescence Efficiency Limitations of Perovskite Light-Emitting Diodes. *Science* **2015**, *350* (6265), 1222−1225.
(32) Park, M. H.; Jeong, S. H.; Seo, H. K.; Wolf, C.; Kim, Y. H.; Kim, H.; Byun, J.; Kim, J. S.; Cho, H.; Lee, T. W. Unravelling Additive-Based Nanocrystal Pinning for High Efficiency Organic-Inorganic Halide Perovskite Light-Emitting Diodes. *Nano Energy* **2017**, *42*, 157−165.
(33) Yu, J.; Wang, N.; Zang, Y.; Jiang, Y. Organic Photovoltaic Cells Based on TPBi as a Cathode Buffer Layer. *Sol. Energy Mater. Sol. Cells* **2011**, *95* (2), 664−668.
(34) Waser, R.; Dittmann, R.; Staikov, G.; Szot, K. Redox-Based Resistive Switching Memories Nanoionic Mechanisms, Prospects, and Challenges. *Adv. Mater.* **2009**, *21* (25−26), 2632−2663.
(35) Sawa, A. Resistive Switching in Transition Metal Oxides. *Mater. Today* **2008**, *11* (6), 28−36.
(36) Han, J. S.; Le, Q. v.; Choi, J.; Kim, H.; Kim, S. G.; Hong, K.; Moon, C. W.; Kim, T. L.; Kim, S. Y.; Jang, H. W. Lead-Free All-Inorganic Cesium Tin Iodide Perovskite for Filamentary and Interface-Type Resistive Switching toward Environment-Friendly and Temperature-Tolerant Nonvolatile Memories. *ACS Appl. Mater. Interfaces* **2019**, *11* (8), 8155−8163.
(37) Tsuruoka, T.; Terabe, K.; Hasegawa, T.; Aono, M. Forming and Switching Mechanisms of a Cation-Migration-Based Oxide Resistive Memory. *Nanotechnology* **2010**, *21* (42), 425205.
(38) Kim, S. G.; van Le, Q.; Han, J. S.; Kim, H.; Choi, M. J.; Lee, S. A.; Kim, T. L.; Kim, S. B.; Kim, S. Y.; Jang, H. W. Dual-Phase All-Inorganic Cesium Halide Perovskites for Conducting-Bridge Memo-

ry-Based Artificial Synapses. *Adv. Funct. Mater.* **2019**, *29* (49), 1906686.

(39) Chang, C. F.; Chen, J. Y.; Huang, G. M.; Lin, T. Y.; Tai, K. L.; Huang, C. Y.; Yeh, P. H.; Wu, W. W. Revealing Conducting Filament Evolution in Low Power and High Reliability Fe3O4/Ta2O5 Bilayer RRAM. *Nano Energy* **2018**, *53*, 871−879.

(40) Lian, X.; Shen, X.; Zhang, M.; Xu, J.; Gao, F.; Wan, X.; Hu, E.; Guo, Y.; Zhao, J.; Tong, Y. Resistance Switching Characteristics and Mechanisms of MXene/SiO2 Structure-Based Memristor. *Appl. Phys. Lett.* **2019**, *115* (6), 063501.

(41) Ding, S.; Wu, Z.; Qu, X.; Tang, H.; Wang, K.; Xu, B.; Sun, X. W. Impact of the Resistive Switching Effects in ZnMgO Electron Transport Layer on the Aging Characteristics of Quantum Dot Light-Emitting Diodes. *Appl. Phys. Lett.* **2020**, *117* (9), 093501.

(42) Wang, H.; Yan, X. Overview of Resistive Random Access Memory (RRAM): Materials, Filament Mechanisms, Performance Optimization, and Prospects. *Phys. Status Solidi RRL* **2019**, *13* (9), 1900073.

(43) Ambrosi, E.; Bricalli, A.; Laudato, M.; Ielmini, D. Impact of Oxide and Electrode Materials on the Switching Characteristics of Oxide ReRAM Devices. *Faraday Discuss.* **2019**, *213*, 87−98.

(44) Zhang, S.; Long, S.; Guan, W.; Liu, Q.; Wang, Q.; Liu, M. Resistive switching characteristics of $MnO_x$-based ReRAM. *J. Phys. D Appl. Phys.* **2009**, *42* (5), 055112.

(45) Park, T. H.; Song, S. J.; Kim, H. J.; Kim, S. G.; Chung, S.; Kim, B. Y.; Lee, K. J.; Kim, K. M.; Choi, B. J.; Hwang, C. S. Thickness-Dependent Electroforming Behavior of Ultra-Thin Ta2O5 Resistance Switching Layer. *Phys. Status Solidi RRL* **2015**, *9* (6), 362−365.

(46) Song, S. J.; Seok, J. Y.; Yoon, J. H.; Kim, K. M.; Kim, G. H.; Lee, M. H.; Hwang, C. S. Real-Time Identification of the Evolution of Conducting Nano-Filaments in TiO2 Thin Film ReRAM. *Sci. Rep.* **2013**, *3*, 3443.

(47) Kim, S. G.; Han, J. S.; Kim, H.; Kim, S. Y.; Jang, H. W. Recent Advances in Memristive Materials for Artificial Synapses. *Adv. Mater. Technol.* **2018**, *3* (12), 1800457.

(48) Hu, Q.; Kang, T. S.; Abbas, H.; Lee, T. S.; Lee, N. J.; Park, M. R.; Yoon, T. S.; Kang, C. J. Resistive Switching Characteristics of Ag/MnO/CeO2/Pt Heterostructures Memory Devices. *Microelectron. Eng.* **2018**, *189*, 28−32.

(49) Rana, A. M.; Akbar, T.; Ismail, M.; Ahmad, E.; Hussain, F.; Talib, I.; Imran, M.; Mehmood, K.; Iqbal, K.; Nadeem, M. Y. Endurance and Cycle-to-Cycle Uniformity Improvement in Tri-Layered CeO2/Ti/CeO2 Resistive Switching Devices by Changing Top Electrode Material. *Sci. Rep.* **2017**, *7*, 39539.

(50) Lee, S. M.; Kim, H.; Kim, D. H.; Kim, W. bin; Lee, J. M.; Choi, J.; Shin, H.; Han, G. S.; Jang, H. W.; Jung, H. S. Tailored 2D/3D Halide Perovskite Heterointerface for Substantially Enhanced Endurance in Conducting Bridge Resistive Switching Memory. *ACS Appl. Mater. Interfaces* **2020**, *12* (14), 17039−17045.

(51) Lin, L. M.; Yang, W. L.; Lin, Y. H.; Hsiao, Y. P.; Chin, F. T.; Kao, M. F. A Novel Nanoscale-Crossbar Resistive Switching Memory Using a Copper Chemical Displacement Technique. *Phys. Status Solidi A* **2017**, *214* (3), 1600595.

(52) Lim, E. W.; Ismail, R. Conduction Mechanism of Valence Change Resistive Switching Memory: A Survey. *Electronics* **2015**, *4* (3), 586−613.

(53) Kim, H.; Choi, M.-J.; Suh, J. M.; Han, J. S.; Kim, S. G.; Le, Q. v.; Kim, S. Y.; Jang, H. W. Quasi-2D Halide Perovskites for Resistive Switching Devices with ON/OFF Ratios above $10^9$. *NPG Asia Mater.* **2020**, *12* (1), 21.

(54) Chen, Y. T.; Chang, T. C.; Peng, H. K.; Tseng, H. C.; Huang, J. J.; Yang, J. B.; Chu, A. K.; Young, T. F.; Sze, S. M. Insertion of a Si Layer to Reduce Operation Current for Resistive Random Access Memory Applications. *Appl. Phys. Lett.* **2013**, *102* (25), 252902.

(55) Tsuruoka, T.; Terabe, K.; Hasegawa, T.; Aono, M. Temperature Effects on the Switching Kinetics of a Cu-Ta $_2$ O $_5$ -Based Atomic Switch. *Nanotechnology* **2011**, *22* (25), 254013.

(56) Liu, D.; Lin, Q.; Zang, Z.; Wang, M.; Wangyang, P.; Tang, X.; Zhou, M.; Hu, W. Flexible All-Inorganic Perovskite $CsPbBr_3$ Nonvolatile Memory Device. *ACS Appl. Mater. Interfaces* **2017**, *9* (7), 6171−6176.

(57) Hwang, B.; Lee, J.-S. A Strategy to Design High-Density Nanoscale Devices Utilizing Vapor Deposition of Metal Halide Perovskite Materials. *Adv. Mater.* **2017**, *29* (29), 1701048.

(58) Hwang, B.; Lee, J.-S. Lead-Free, Air-Stable Hybrid Organic-Inorganic Perovskite Resistive Switching Memory with Ultrafast Switching and Multilevel Data Storage. *Nanoscale* **2018**, *10* (18), 8578−8584.

(59) Lee, S.; Wolfe, S.; Torres, J.; Yun, M.; Lee, J.-K. Asymmetric Bipolar Resistive Switching of Halide Perovskite Film in Contact with $TiO_2$ Layer. *ACS Appl. Mater. Interfaces* **2021**, *13* (23), 27209−27216.

(60) Yoo, E. J.; Lyu, M.; Yun, J.-H.; Kang, C. J.; Choi, Y. J.; Wang, L. Resistive Switching Behavior in Organic-Inorganic Hybrid $CH_3NH_3PbI_{3-x}Cl_x$ Perovskite for Resistive Random Access Memory Devices. *Adv. Mater.* **2015**, *27* (40), 6170−6175.

(61) Ge, S.; Guan, X.; Wang, Y.; Lin, C.; Cui, Y.; Huang, Y.; Zhang, X.; Zhang, R.; Yang, X.; Wu, T. Low-Dimensional Lead-Free Inorganic Perovskites for Resistive Switching with Ultralow Bias. *Adv. Funct. Mater.* **2020**, *30* (25), 2002110.

(62) Ge, S.; Huang, Y.; Chen, X.; Zhang, X.; Xiang, Z.; Zhang, R.; Li, W.; Cui, Y. Silver Iodide Induced Resistive Switching in $CsPbI_3$ Perovskite-Based Memory Device. *Adv. Mater. Interfaces* **2019**, *6* (7), 1802071.

(63) Xia, F.; Xu, Y.; Li, B.; Hui, W.; Zhang, S.; Zhu, L.; Xia, Y.; Chen, Y.; Huang, W. Improved Performance of $CH_3NH_3PbI_{3-x}Cl_x$ Resistive Switching Memory by Assembling 2D/3D Perovskite Heterostructures. *ACS Appl. Mater. Interfaces* **2020**, *12* (13), 15439−15445.

(64) Zeng, F.; Tan, Y.; Hu, W.; Tang, X.; Luo, Z.; Huang, Q.; Guo, Y.; Zhang, X.; Yin, H.; Feng, J.; Zhao, X.; Yang, B. Impact of Hydroiodic Acid on Resistive Switching Performance of Lead-Free $Cs_3Cu_2I_5$ Perovskite Memory. *J. Phys. Chem. Lett.* **2021**, *12* (7), 1973−1978.

(65) Paramanik, S.; Maiti, A.; Chatterjee, S.; Pal, A. J. Large Resistive Switching and Artificial Synaptic Behaviors in Layered $Cs_3Sb_2I_9$ Lead-Free Perovskite Memory Devices. *Adv. Electron. Mater.* **2022**, *8* (1), 2100237.

(66) Cheng, P.; Zhu, Y.; Shi, J.; Wang, H.; Liu, Y.; Xiong, R.; Wei, J.; Ma, H.; Yin, M. One-Step Solution Deposited All-Inorganic Perovskite $CsPbBr_3$ Film for Flexible Resistive Switching Memories. *Appl. Phys. Lett.* **2019**, *115* (22), 223505.

(67) Chen, R.; Xu, J.; Lao, M.; Liang, Z.; Chen, Y.; Zhong, C.; Huang, L.; Hao, A.; Ismail, M. Transient Resistive Switching for Nonvolatile Memory Based on Water-Soluble $Cs_4PbBr_6$ Perovskite Films. *Phys. Status Solidi RRL* **2019**, *13* (11), 1900397.

(68) Wang, H.; Lin, J.; Zhu, Y.; Zeng, X.; Wei, H.; Cheng, P.; Lu, H.; Liu, Y.; Xiong, R. Fabrication of Flexible Resistive Switching Devices Based on Lead-Free All-Inorganic $CsSnBr_3$ Perovskite Using a One-Step Chemical Vapor Deposition Method. *Adv. Electron. Mater.* **2020**, *6* (11), 2000799.

(69) Cuhadar, C.; Kim, S.-G.; Yang, J.-M.; Seo, J.-Y.; Lee, D.; Park, N.-G. All-Inorganic Bismuth Halide Perovskite-Like Materials $A_3Bi_2I_9$ and $A_3Bi_{1.8}Na_{0.2}I_{8.6}$ (A = Rb and Cs) for Low-Voltage Switching Resistive Memory. *ACS Appl. Mater. Interfaces* **2018**, *10* (35), 29741−29749.



https://doi.org/10.1021/acsami.3c01450
ACS Appl. Mater. Interfaces XXXX, XXX, XXX−XXX